Ab Initio Molecular-Dynamics Simulations of Short-Range Order in Liquid $Al_{80}Mn_{20}$ and $Al_{80}Ni_{20}$ Alloys

N. Jakse

Laboratoire de Théorie de la Matière Condensée, Université de Metz, 1. Boulevard FD Arago, 57078 Metz Cedex 3, France

O. Lebacq and A. Pasturel

Laboratoire de Physique et Modélisation des Milieux Condensés, Maison des Magistères,
BP 166 CNRS, 38042 Grenoble-Cedex 09, France
(Received 26 June 2004; published 9 November 2004)

Atomic structures of liquid $Al_{80}Mn_{20}$ and $Al_{80}Ni_{20}$ have been calculated by first-principles molecular-dynamics simulations. For both liquid alloys, the local structure is characterized by a strong Al-TM (transition metal) affinity, which leads to a well-pronounced chemical short-range order. However, we show that the occurrence of magnetic moments localized on Mn atoms plays a key role in determining the short-range arrangement of Mn atoms which is also interpreted on the basis of the local fivefold symmetry.

The nature of short-range structure is essential to understand the special properties of metallic liquids and glasses [1]. For close-packed systems, the icosahedron cluster has been proposed to be an important building block, which becomes predominant during liquid quenching according to Frank's suggestions [2]. With the discovery by Shechtman *et al.* [3] of quasiperiodic structures with icosahedral symmetry, many experimental attempts [4–7] have been made to study the local order in liquid alloys forming quasicrystalline phases such as those based on Al-TM (transition metal) alloys. For such alloys, the overall similarity observed between the structure factors of liquid phases and their parent icosahedrally coordinated quasicrystalline phases has been taken as proof, albeit indirect, that the fivefold symmetry also exists over short range in the liquid phases. For Mn-based alloys, the appearance of localized moments in the liquid state [5] makes such experimental analysis still more difficult since it is generally thought that the formation of local magnetic moments is not related to icosahedral site symmetry [8].

Molecular-dynamics (MD) simulations offer an alternate possibility to determine the short-range structure in liquids. However, an accurate simulation of the properties of Al-TM alloys is still a challenging problem since bonding is not well described by currently available pair and embedded-atom potentials. For instance, the model structure for the liquid $Al_{86}Mn_{14}$ alloy prepared by molecular-dynamics simulations using either pair potentials proposed by Phillips *et al.* [9] or interatomic potentials based on a semiempirical tight-binding approach [10] lead to different descriptions of its magnetic property [8,11]. To further clarify the short-range order in liquid Al-TM alloys, we have undertaken a study of structural properties of liquid $Al_{80}Mn_{20}$ and $Al_{80}Ni_{20}$ alloys based upon first-principles molecular-dynamics simulations.

The interest of such a study is to differentiate and characterize the local structure motifs in the quasicrystal-forming liquid $Al_{80}Mn_{20}$ and in the liquid $Al_{80}Ni_{20}$, from which no quasicrystalline phase evolves. For both liquids, our findings show that the local structure is characterized by a strong Al-TM affinity, which leads to a well-pronounced chemical short-range order (SRO). However, we demonstrate that the occurrence of magnetic moments localized on Mn atoms plays a key role in determining their local environments. From structural analysis using bonding orientational order and three-dimensional pair analysis techniques, the icosahedral short-range order is evidenced in $Al_{80}Mn_{20}$ as opposed to what occurs in $Al_{80}Ni_{20}$.

We have carried out first-principles simulations of liquid $Al_{80}Mn_{20}$ and alloys using the *ab initio* total-energy and molecular-dynamics program VASP [12] in which the interactions between the ions and electrons are described by the projector augmented-wave method [13]. Simulations were performed using a gradient corrected energy functional [14] and a plane-wave cutoff of 270 eV for both alloys. In the simulations for $Al_{80}Mn_{20}$, we have treated the spin variable explicitly with the gradient corrected local spin density approximation [15]. We have considered a system of 205 Al atoms and 51 TM atoms in a cubic box with periodic boundary conditions such that the densities of the two systems reproduce the experimental ones [4]. Only the Γ-point sampling was considered to sample the supercell Brillouin zone. The initial positions are extracted from tight-binding molecular-dynamics simulations [10] and all the dynamical simulations were carried out in the canonical ensemble by means of a Nosé thermostat with a characteristic frequency equal to 38 ps^{-1}. The simulated temperatures were those of the experiments, namely, $T = 1380$ K and $T = 1320$ K for $Al_{80}Mn_{20}$ and $Al_{80}Ni_{20}$, respectively (about 60 K above

their experimental liquidus temperatures). Newton's equations of motion were integrated using the Verlet algorithm with a time step of 3 fs. For each alloy, the total simulation time was 7.5 ps, which followed a 1.5 ps equilibration phase.

The Bhatia-Thorton partial structure factors shown in Fig. 1 are based on averages of over 100 independent configurations. They are perfectly in phase with the experimental curves and, more particularly, reproduce quite well the experimental height of the first and second peaks of $S_{NN}(q)$ for both $Al_{80}Mn_{20}$ and $Al_{80}Ni_{20}$ liquids. The largest difference between both liquids is undoubtedly in the height and the shape of the first peak of $S_{NN}(q)$ [$S_{NN}(q_1) = 1.90$ with $q_1 = 2.95$ Å^{-1} for $Al_{80}Ni_{20}$ and $S_{NN}(q_1) = 2.25$ with $q_1 = 2.85$ Å^{-1} for $Al_{80}Mn_{20}$]. As already discussed [4], such a change can be attributed to a variation of the special extent of topological ordering, the atoms in $Al_{80}Mn_{20}$ being arranged roughly over one more interatomic distance than in $Al_{80}Ni_{20}$. Our simulations also reproduce the pronounced peak in the chemical-chemical structure factor [$S_{CC}(q)$], indicative of a well-defined chemical SRO in both liquids. In agreement with experiments, the first and second oscillations of the two functions are comparable in amplitude, but those

FIG. 1. Bhatia-Thornton partial structure factors for $Al_{80}Mn_{20}$ (a) and $Al_{80}Ni_{20}$ (b) liquids. Triangles, circles, and squares correspond, respectively, to the experimental $S_{NN}(q)$, $S_{NC}(q)$, and $S_{CC}(q)$ from Ref. [4]. The solid lines represent the corresponding partial structure factors from the MD simulations.

for $Al_{80}Ni_{20}$ are shifted towards higher q. For $Al_{80}Ni_{20}$ let us mention that our results are comparable to that obtained by Asta et al. [16].

Table I lists the structural parameters related to the first and second coordination shells in $Al_{80}Ni_{20}$ and $Al_{80}Mn_{20}$ liquids together with the corresponding experimental ones [4] for comparison. Concerning $Al_{80}Ni_{20}$ liquid, the experimental hierarchy of the bond lengths is well reproduced; i.e., the Ni-Al bond length is significantly smaller than the values of Ni-Ni and Al-Al bond lengths. Our results are in better agreement with experimental results than those obtained by Asta et al., partly due to different exchange and correlation functionals since the over-binding given by local density approximation is largely corrected by generalized gradient approximation for metallic alloys. For $Al_{80}Mn_{20}$ liquid, it has been experimentally shown that a localized moment appears on Mn atoms in the liquid state, giving rise to a remarkable evolution of the susceptibility as a function of temperature [5]. Therefore, magnetic interactions may not be ignored and an explicit spin treatment for the structural properties of $Al_{80}Mn_{20}$ liquid has been included in our MD simulation as mentioned above. As shown in Table I, the experimental bond lengths are well reproduced. To emphasize the role played by magnetic interactions, we have also performed MD simulations by omitting the spin treatment. In this case, if calculations are able to reproduce the experimental Al-Al and Al-Mn bond lengths, they fail to reproduce the first distances Mn-Mn. Therefore, the quantitative difference (as large as 20%) can be attributed to an incorrect description of Mn-Mn interactions To confirm this analysis, we show in Fig. 2 $G_{MnMn}(r)$ calculated with and without explicit treatment of spin. The two curves are found to be very different both in the location and the height of the first and second peaks, spin effects leading to a correct description of
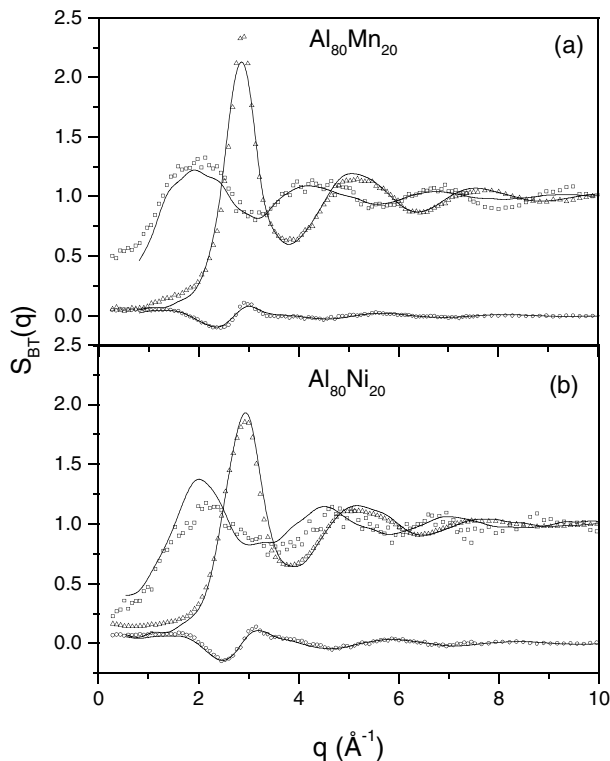
TABLE I. Positions of first and second peaks of the partial TM-TM, Al-TM, and Al-Al pair-correlation functions in $Al_{80}Mn_{20}$ and $Al_{80}Ni_{20}$ liquids, where TM means the transition element considered. Columns (MD) and (expt.) correspond, respectively, to the MD simulations of the present work and the experimental parameters from Ref. [4]. The values in parenthesis for $Al_{80}Mn_{20}$ are the distances without the explicit spin treatment.

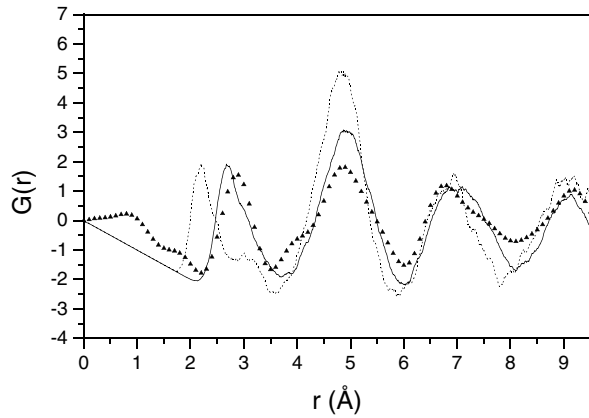|	$Al_{80}Ni_{20}$		$Al_{80}Mn_{20}$	
	r_{ij} (Å) (MD)	r_{ij} (Å) (Expt.)	r_{ij} (Å) (MD)	r_{ij} (Å) (Expt.)
TM-TM	2.67	2.63	2.85 (2.30)	2.89
	4.51	4.60	4.95 (4.85)	4.85
Al-TM	2.47	2.54	2.60 (2.55)	2.56
	4.65	4.48	4.85 (4.80)	4.6
Al-Al	2.77	2.82	2.76 (2.76)	2.74
	5.00	4.9−5.7	5.00 (5.00)	4.8−5.3

FIG. 2. Mn-Mn partial pair-correlation function $G_{\text{Mn-Mn}}(r)$ from the MD simulations with (solid line) and without (dashed lines) magnetic interactions. The symbols correspond to the experimental curve of Ref. [4].

FIG. 3. Bond-angle distributions for $Al_{80}Mn_{20}$ (solid lines) and $Al_{80}Ni_{20}$ (dotted lines) liquids. The thick lines correspond to the total distribution, while the thin lines are the partial distributions around the transition elements.

the experimental partial pair-correlation function. We have checked that our results do not depend on the initial magnetic configuration. Our results show that magnetic interactions are the driving mechanism to obtain a correct description of the Mn-Mn distribution. Such a contribution ignored in previous theoretical approaches may explain their inability to provide a quantitative description of the magnetic properties of liquid Al-Mn alloys.

The comparison of the partial functions determined for the $Al_{80}Mn_{20}$ and $Al_{80}Ni_{20}$ alloys shows that the local structure motifs, defined by the set of the interatomic distances given in Table I, are different. Indeed, we find r_{MM} equal to 2.67 Å in $Al_{80}Ni_{20}$, while it is equal to 2.85 Å in $Al_{80}Mn_{20}$. This difference cannot be attributed to the very small atomic size difference between Ni and Mn atoms and suggests that the local arrangements are different. This is also supported by the first Al-Al distances which are significantly shorter than Mn-Mn contacts in $Al_{80}Mn_{20}$ and greater than Ni-Ni contacts in $Al_{80}Mn_{20}$. The fact that the topological short-range order is different in both alloys is also confirmed by the bond-angle distribution functions drawn in Fig. 3. In a tetrahedrally close-packed structure, the bond-angle distribution $g(\theta)$ has two peaks at the icosahedral bond angles ($t = 63.5°$ and $t = 116.5°$), and this distribution is only slightly changed if systems with larger size ratios are considered. For both alloys, the bond angles around the Al atoms are quite similar, but characteristic differences are found in the bonds centered at TM atoms. Indeed, the partial bond-angle distribution functions show that the surrounding of the Mn atoms is essentially icosahedral whereas it is not the case around the Ni atoms, the bond angles being far from the values of the icosahedron.

To obtain more detailed information about the local atomic structure of the $Al_{80}Mn_{20}$ and $Al_{80}Ni_{20}$ alloys, we use the common-neighbor (CN) analysis [17] that decomposes the partial pair-correlation functions according to

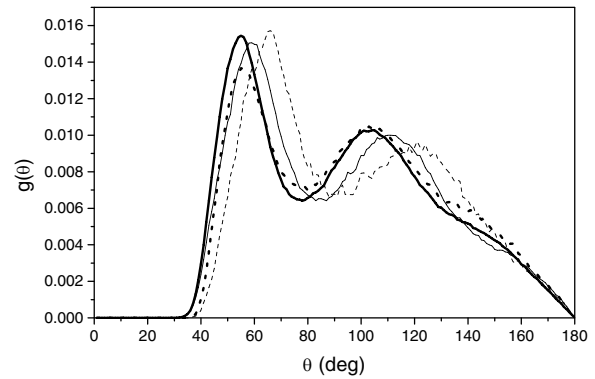the different local environment of the bonded pairs. This method is able to characterize the local environment surrounding each atomic pair that contributes to the peaks of the pair-correlation functions, in terms of the number and properties of common nearest neighbors of the pair under consideration. Such an analysis is performed on inherent structures in which the atoms are brought to local minima of the potential energy surface by applying a technique similar to the steepest-descent minimization proposed by Stillinger and Weber [18]. For each alloy, ten selected configurations regularly spaced in time are used to generate the corresponding inherent structures from which an average relative abundance of selected pairs is determined and gathered in Table II. More particularly, the CN analysis was also applied to the pairs involving at least one transition metal atom since the partial bond-angle distribution functions display different surroundings of the transition metal atoms. This method, which can distinguish between the fcc, hcp, bcc, and icosahedral packing, is described in more details in Ref. [19].

The microscopic analysis emerging from the data of Table II confirms that the local environment of Mn atoms is quite different from that of Ni atoms. The local environment of Mn atoms is dominated by icosahedral and distorted icosahedral inherent structures since the 1551 and 1541 bonded pairs are preponderant. Their sum amounts to more than 50% of the total number of all bond types whereas only 35% of 1441, 1431, 1421 and 1422 pairs, related to the tetrahedral local order, are found. However, although the 2331 pairs are relatively numerous, the absence of the 1321 pairs and the presence of the 1661 ones is a strong indication that the local order is more complex than the one found in the 13-atom icosahedron [19]. Let us mention that the relative numbers of 1331, 1321, 1311, and 1301, related to the rhombohedral structures, represent only a small fraction of all bonded pairs. In $Al_{80}Ni_{20}$ our findings are quite different since the 1441, 1431, 1421,

TABLE II. Analysis of the MD simulations in bonded pairs for $Al_{80}Ni_{20}$ and $Al_{80}Mn_{20}$ liquids. The columns named total correspond to the analysis of all the pairs in the system while the columns named Ni and Mn are partial analysis of the pairs in which at least one of the atoms is Ni and Mn, respectively. The abundances are averaged over the ten selected inherent configurations and the absolute error bars of the abundances is 0.01.

Pairs	$Al_{80}Ni_{20}$ Total	Ni	$Al_{80}Mn_{20}$ Total	Mn
1551	0.14	0.25	0.18	0.37
1541	0.15	0.10	0.14	0.13
1431	0.25	0.34	0.21	0.21
1421	0.05	0.04	0.03	0.02
1422	0.10	0.07	0.10	0.05
1201	0.02	0.00	0.03	0.00
1211	0.01	0.00	0.01	0.00
1301	0.02	0.01	0.02	0.00
1311	0.10	0.06	0.08	0.02
1321	0.06	0.04	0.07	0.02
1331	0.00	0.00	0.00	0.00
1441	0.03	0.07	0.04	0.08
1661	0.03	0.01	0.03	0.06
1771	0.00	0.00	0.00	0.00
1881	0.00	0.00	0.00	0.00
2101	1.81	1.96	1.75	1.71
2211	1.00	1.17	0.93	1.08
2321	0.18	0.10	0.15	0.06
2331	0.59	0.65	0.64	0.76
2441	0.13	0.08	0.13	0.11

and 1422 pairs become preponderant. The sum of these four types of pairs amounts to more than 50% of the total number of all bond types, indicating a strong tetrahedral local order. On the contrary, the 1551 and 1541 bond types, related to the icosahedral configuration, contributes to only 34.3% of the total number of all bond types. Such a result indicates that the icosahedral packing is still present in $Al_{80}Ni_{20}$ but strongly hidden by the tetrahedral packing.

To summarize, we have performed *ab initio* MD simulations of liquid $Al_{80}Mn_{20}$ and $Al_{80}Ni_{20}$ alloys in order to analyze their local order. The structure of $Al_{80}Ni_{20}$ liquid, characterized through the Bhatia-Thorton partial structure factors and the partial pair-correlation functions, was found to be in very good agreement with experimental data. For $Al_{80}Mn_{20}$ liquid, we have shown that an explicit spin treatment is necessary to obtain a correct description of the Mn-Mn distribution. This result predicted by our simulations differs from those found in previous classical and empirical models. A more refined structural analysis, using a method to classify inherent structures, allows one to gain additional insight into the atomic configurations characterizing the SRO found in the two liquid alloys. In $Al_{80}Mn_{20}$, the analysis clearly

points out the predominance of the fivefold symmetry around Mn atoms. On the contrary, in $Al_{80}Ni_{20}$, the local environment of Ni atoms is characterized by the predominance of the close-packed local symmetry over the icosahedral symmetry. Our results can be viewed as a proof that the fivefold symmetry is preponderant in the liquid alloys from which quasicrystalline phases may be formed by quenching techniques.

[1] D. R. Nelson and F. Spaepen, *Solid State Physics*, edited by H. Ehrenreich, F. Seitz, and D. Turnbull (Academic, New York, 1989), Vol. 42, p. 1.
[2] F. C. Frank, Proc. R. Soc. London A **215**, 43 (1952).
[3] D. Shechtman, I. Blech, D. Gratias, and J. W. Cahn, Phys. Rev. Lett. **53**, 1951 (1984).
[4] M. Maret, A. Pasturel, C. Senillou, J. M. Dubois, and P. Chieux, J. Phys. (Paris) **50**, 295 (1989); M. Maret, T. Pomme, A. Pasturel, and P. Chieux, Phys. Rev. B **42**, 1598 (1990); M. Maret, P. Chieux, J. M. Dubois, and A. Pasturel, J. Phys. Condens. Matter **3**, 2801 (1991).
[5] F. Hippert, M. Audier, H. Klein, R. Bellissent, and D. Boursier, Phys. Rev. Lett. **76**, 54 (1996).
[6] V. Simonet, F. Hippert, H. Klein, M. Audier, R. Bellissent, H. Fischer, A. P. Murani, and D. Boursier, Phys. Rev. B **58**, 6273 (1998); V. Simonet, F. Hippert, M. Audier, and R. Bellissent, Phys. Rev. B **65**, 024203 (2001).
[7] T. Schenk, V. Simonet, D. Holland-Moritz, R. Bellissent, T. Hansen, P. Convert, and D. M. Herlach, Europhys. Lett. **65**, 34 (2004).
[8] J. Hafner and M. Krajci, Phys. Rev. B **57**, 2849 (1998).
[9] R. Phillips, J. Zou, A. C. Carlsson, and M. Widom, Phys. Rev. B **49**, 9322 (1994).
[10] L. D. Phuong, D. Nguyen Manh, and A. Pasturel, Phys. Rev. Lett. **71**, 372 (1993).
[11] A. M. Bratkovsky, A. V. Smirnov, D. Nguyen Manh, and A. Pasturel, Phys. Rev. B **52**, 3056 (1995).
[12] G. Kresse and J. Furthmüller, Comput. Mater. Sci. **6**, 15 (1996); Phys. Rev. B **54**, 11 169 (1996).
[13] G. Kresse and D. Joubert, Phys. Rev. B **59**, 1758 (1999).
[14] Y. Wang and J. P. Perdew, Phys. Rev. B **44**, 13 298 (1991).
[15] S. H. Vosko, L. Wilk, and M. Nusair, Can. J. Phys. **58**, 1200 (1980).
[16] M. Asta, V. Ozolins, J. J. Hoyt, and M. van Schilfgaarde, Phys. Rev. B **64**, R20 201 (2001).
[17] J. D. Honeycutt and H. C. Andersen, J. Phys. Chem. **91**, 4950 (1987).
[18] F. H. Stillinger and T. A. Weber, Phys. Rev. A **25**, 978 (1982).
[19] N. Jakse and A. Pasturel, Phys. Rev. Lett. **91**, 195501 (2003); J. Chem. Phys. **120**, 6124 (2004).